INT. J. NUM. METH. HEAT FLUID FLOW, VOL. 5, 175–183 (1995)

NUMERICAL PREDICTION OF FULLY DEVELOPED TURBULENT SWIRLING FLOWS IN AN AXIALLY ROTATING PIPE BY MEANS OF A MODIFIED k–ε TURBULENCE MODEL

SHUICHI TORII

Department of Mechanical Engineering, Kagoshima University, 1-21-40 Korimoto, Kagoshima 890, Japan

AND

WEN-JEI YANG

Department of Mechanical Engineering and Applied Mechanics, University of Michigan, Ann Arbor, Michigan 48109, USA

ABSTRACT

A numerical study is performed to investigate turbulent flow characteristics in a pipe rotating around the axis. Emphasis is placed on the effect of pipe rotation on the friction coefficient and velocity distribution in the hydrodynamically, fully-developed flow region. The k–ε turbulence model is modified by taking the swirling effect into account, in which the model function including the Richardson number is introduced to the ε equation. The governing boundary-layer equations are discretized by means of a control volume *finite*-difference technique for numerical computation. Results obtained from the modified model agree well with experiment data in the existing literature. It is found from the study that (i) an axial rotation of the pipe induces an attenuation in the turbulent kinetic energy, resulting in a reduction in the friction coefficient, and (ii) an increase in the velocity ratio causes substantial decreases in the friction coefficient, the turbulent kinetic energy and the streamwise velocity gradient near the wall.

KEY WORDS Turbulent swirling flows Finite difference method Rotating pipe

NOMENCLATURE

C_μ, C_1, C_2	empirical constants in k–ε model	k	turbulent kinetic energy, $(\overline{u'^2} + \overline{v'^2} + \overline{w'^2})/2$, m^2/s^2
C_3	model function in k–ε model, (12) and (14)	N	velocity ratio, W/U
d	in diameter, m	P	time-averaged pressure, Pa
D	modification term in the wall region, in (7)	Pr	Prandtl number
		r	radial coordinate, m
E	modification term in the wall region, in (8)	Re	Reynolds number
		Ri	Richardson number, (13)
f	friction coefficient	R_t	turbulent Reynolds number, $k^2/\varepsilon\nu$
f_μ, f_1, f_2	turbulent model functions in k–ε model	R_τ	dimensionless distance in radial direction, u^*y/ν

0961–5539/95/020175–09$2.00

Received May 1993
Revised January 1994

U	mean axial velocity across tube cross section, m/s
$\bar{u}$, $\bar{v}$, $\bar{w}$	time-averaged velocity components in axial, radial and tangential directions, respectively, m/s
u', v', w'	fluctuating velocity components in axial, radial and tangential directions, respectively, m/s
u^*	friction velocity, m/s
W	tangential velocity on the wall
x	axial coordinate, m
y	distance from the wall, m
z^*	dimensionless length, $x/(d/2)$

Greek letters

θ	coordinate in tangential direction
ε	turbulent energy dissipation rate, m^2/s^3
ν, ν_t	molecular and turbulent viscosities, m^2/s
σ_k, σ_ε	turbulent Prandtl numbers for k and ε, respectively

Subscripts

max	maximum
o	no rotation

Superscripts

	time-averaged value
	fluctuation value

INTRODUCTION

The problems of fluid flow and heat transfer in axially rotating pipes are encountered in the inlet part of fluid machinery, rotating heat exchangers and cooling systems of rotors. They are of considerable theoretical interest and have important applications in the power and refrigeration industries. When a fluid enters a pipe rotating around its axis, the tangential force induced by rotation produces a fluid swirl, resulting in a proper flow pattern, which is a sharp contrast to that in a stationary pipe. Numerical and experimental investigations pertinent to these phenomena are available in the literature. Some references are cited below, which are relevant to the present study.

Murakami *et al.*[1] measured the time-averaged streamwise and tengential velocity components and hydraulic losses in axially rotating pipes into which a fully developed turbulent flow was introduced. It was disclosed that the turbulence in the flow and the hydraulic loss are remarkably reduced due to the pipe rotation and that the streamwise velocity approaches a laminar one with an increase in its speed. Such a turbulence suppression was confirmed by the experimental work of Yamada *et al.*[2] and also by the flow visualization study of Cannon and Kays[3].

In order to further understand swirling flow phenomena, Koosinlin *et al.*[4], Aguilar and Pierce[5] and Launder *et al.*[6] analyzed the boundary layer flow developed outside a rotating body by means of a modified mixing length theory, an eddy viscosity model and a two-equation turbulence model, respectively. As to the corresponding flow developed inside a rotating cylinder, Kikuyama *et al.*[7] predicted the streamwise velocity distribution in the fully developed region of a rotating pipe by means of a modified mixing length theory proposed by Bradshaw[8]. Based on the experiment data of Murakami and Kikuyama[1] and Kikuyama *et al.*[17], a parabolic distribution was assumed as the tangential velocity in the theory. Hirai *et al.*[9] reproduced the laminar-flow velocity profiles and the remarkable reduction of the friction factor due to the swirl by means of a Reynolds stress turbulence model. They concluded that these flow behaviours are ascribed to a decrease in the Reynolds stress. It was also pointed out that these flow characteristics cannot be predicted by a standard k–ε turbulence model. In order to overcome this shortcoming, Kawamura and Mishima[10] modified the k–ε model with the aid of the Reynolds stress model to predict the laminarization phenomenon and the tangential velocity profile in the swirling flow.

The knowledge of turbulence structure in an axially rotating pipe flow is essential to the understanding of swirling flow phenomena. However, the existing experimental literature

treats only friction coefficient, time-averaged velocity and Reynolds stress. It postulated the anisotropy of turbulence to be induced by pipe rotation based on a few data on turbulence structure, i.e. three components of normal stresses. For the analysis of a strong anisotropic flow, the Reynolds stress turbulence model is considered a promising model. Although the conventional k–ε model is popularly used in treating engineering problems due to its simplicity and less computational time, is may not accurately predict the anisotropy of turbulent intensities because of the assumption of isotropic turbulence structure. In treating an anisotropic flow induced by pipe rotation, the number of flow quantities in the Reynolds stress model far exceeds that in the k–ε model. Swirling flow phenomena may be elucidated to certain extent by means of the conventional k–ε model, if no precise prediction of flow structure is needed. In order words, the conventional k–ε model based on an isotropic eddy-viscosity representation of the Reynolds stress is still useful in treating flow and heat transfer problems in axially rotating pipes.

The present study treats transport phenomena in the hydrodynamically, fully-developed flow region of an axially rotating pipe. Emphasis is placed on the effect of pipe rotation on the flow structure. Modifications of the two-equation k–ε model are proposed to take the swirling effect into account and to reproduce the existing experimental data. This modified version is then employed to aid in disclosing changes in the radial distributions of velocity and turbulent kinetic energy due to rotation.

THEORETICAL ANALYSIS

Governing equations

The system to be studied is depicted in *Figure 1*. A boundary layer approximation is employed in the analysis of a hydrodynamically, fully-developed turbulent flow through a pipe rotating around its axis. The governing equations in a cylindrical coordinate can be expressed as:

Continuity equation:

$$\frac{\partial \bar{u}}{\partial x} = 0 \tag{1}$$

Momentum equations:

x direction:

$$-\frac{1}{\rho}\frac{\mathrm{d}\bar{P}}{\mathrm{d}x} + \frac{1}{r}\frac{\partial}{r\partial r}\left(rv\frac{\partial \bar{u}}{\partial r} - r\overline{u'v'}\right) = 0 \tag{2}$$

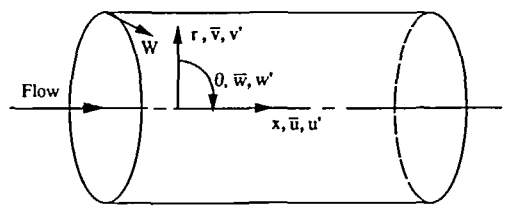

Figure 1 Coordinate system

θ direction:

$$\frac{1}{r^2}\frac{\partial}{\partial r}\left\{r^3\nu\frac{d\left(\frac{\bar{w}}{r}\right)}{\partial r}-r^2\overline{v'w'}\right\}=0 \tag{3}$$

The Reynolds stresses $-\overline{u'v'}$ and $-\overline{v'w'}$ in (2) and (3) are expressed by Boussinesq's approximation as:

$$-\overline{u'v'}=\nu_t\frac{\partial\bar{u}}{\partial r} \tag{4}$$

$$-\overline{v'w'}=\nu_t r\frac{\partial\left(\frac{\bar{w}}{r}\right)}{\partial r} \tag{5}$$

The turbulent viscosity ν_t is related to the turbulent kinetic energy k and its dissipation rate ε through Kolmogorov–Prandtl's relation[11] as:

$$\nu_t=C_\mu f_\mu\frac{k^2}{\varepsilon} \tag{6}$$

In order to evaluate k and ε in (6), a low Reynolds number version of a k–ε turbulence model is used in the present study. Both transport requestions are written as:

$$\frac{1}{r}\frac{\partial}{\partial r}\left\{r\left(\frac{\nu_t}{\sigma_k}+\nu\right)\frac{\partial k}{\partial r}\right\}+\nu_t\left[\left(\frac{\partial\bar{u}}{\partial r}\right)^2+\left\{r\frac{\partial}{\partial r}\left(\frac{\bar{w}}{r}\right)\right\}^2\right]-\varepsilon+D=0 \tag{7}$$

$$\frac{1}{r}\frac{\partial}{dr}\left\{r\left(\frac{\nu_t}{\sigma_\varepsilon}+\nu\right)\frac{\partial\varepsilon}{\partial r}\right\}+C_1f_1\frac{\varepsilon}{k}\nu_t\left[\left(\frac{\partial\bar{u}}{\partial r}\right)^2+\left\{r\frac{\partial}{\partial r}\left(\frac{\bar{w}}{r}\right)\right\}^2\right]-C_2C_3f_2\frac{\varepsilon^2}{k}+E=0 \tag{8}$$

In solving a series of the governing equations, only one-half of the pipe cross-section is treated because of the symmetry in the fluid flow. Thus, the boundary conditions are specified as:

at r = *0 (centreline)*:

$$\frac{\partial\bar{u}}{\partial r}=\frac{\partial\bar{w}}{\partial r}=\frac{\partial k}{\partial r}=\frac{\partial\varepsilon}{\partial r}=0,\qquad \bar{w}=0$$

at r = d/*2 (wall)*:

$$\bar{u}=k=\varepsilon=0,\qquad \bar{w}=W(\text{tangential velocity})$$

Discussion on a k–ε *turbulence model and modification*

As revealed in the previous section, Kirai *et al.*[9] reported that if the standard k–ε model is applied to an axially rotating pipe flow, there would be no distinction between the calculated streamwise velocity distributions without and with rotation and turbulence suppression of the swirling flow by the centrifugal force (so-called laminarization phenomena) would not occur. This is attributed to a linear radial profile of the tangential velocity, as pointed out by Kawamura and Mishima[10]. This relationship is presented in the Appendix. The linear tangential velocity distribution does not impose the swirling effect in the production terms of the k and ε equations, i.e. (7) and (8), which do not have the term for reducing the turbulent kinetic energy due to the swirling. In order to predict swirling flow phenomena in an axially rotating pipe, it is necessary to prescribe the swirl velocity profile and to modify the k or ε equations as follows:

Kikuyama *et al.*[7] found that both Reynolds number and rotation rate do not affect the radial profiles of the time-averaged tangential velocity at different axial locations. This observation was confirmed by Weigand and Beer[12] who proposed that the universal tangential profile depends on the radial location and the axial distance from the inlet as:

$$\bar{w} = W\left(\frac{r}{d/2}\right)^{(2+f(z^*))} \tag{9}$$

where

$$f(z^*) = \frac{1}{z^*} + 9.5e^{-0.019z^*} \tag{10}$$

In the hydrodynamically, fully-developed flow region, (9) can be reduced as:

$$\bar{w} = W\left(\frac{r}{d/2}\right)^2 \tag{11}$$

In the present study, (11) is employed to replace (3) in determining the tangential velocity.

In the study of turbulent shear flows on rotating or curved surfaces, Launder *et al.*[6] proposed a modified k–ε turbulence model to include the curvature effect by adjusting C_3 in the dissipation term of the turbulence dissipation rate equation, (8). It yields a model function containing a Richardson number, Ri, as:

$$C_3 = 1 - 0.2Ri, \tag{12}$$

where

$$Ri = \frac{k^2}{\varepsilon^2}\frac{\bar{w}}{r^2}\frac{\partial(r\bar{w})}{\partial r} \tag{13}$$

This modified k–ε model proposed by Launder *et al.*[6] was first applied to an axially rotating pipe flow to determine swirling effects. It predicts rotation to induce more severe amplification of the laminarizing flow than actual experimental data, as will be seen in the succeeding section. The reason is that as the tangential velocity is increased (i.e. an increase in Ri), the term with C_3 in (8) amplifies the level of ε, resulting in a reduction in the turbulent kinetic energy. Note that no such effect would appear if a linear tangential velocity is used (as mentioned previously). Now, C_3 is optimized to obtain the desired performance utilizing a trial-and-error process (by varying the constant and exponent of the Richardson number in (12) in the ranges of $0.01 \sim 1.0$ and of $0.1 \sim 2.0$, respectively). The modified version is derived as:

$$C_3 = 1 - 0.06Ri^{0.5} \tag{14}$$

The conventional k–ε turbulence model has been employed by many investigators with different empirical constants and model functions. No appreciable difference was gained even the wall limiting behaviour was taken into consideration in the modelling. Torii *et al.*[13] used several existing k–ε models to determine flow and heat transfer characteristics in both isothermal and slightly heated flows without rotation, yielding practically the same results. In the present study, the k–ε models proposed by Launder and Sharma[14], Nagano and Hishida[15], and Torii *et al.*[13] are employed. The model function, (14), is adapted in each of these models to induce the swirling effect. The original model of Launder *et al.*[6] is also included for comparison. The empirical constants and model functions in (6), (7) and (8) are summarized in *Table 1* for the four turbulence models.

Table 1 Empirical constants and model functions

	Launder & Sharma[14]	Nagano & Hishida[15]	Torii *et al.*[13]	Launder *et al.*[6]
C_μ	0.09	0.09	0.09	0.09
C_1	1.45	1.45	1.44	1.45
C_2	2.0	1.9	1.9	2.0
C_3	1.0	1.0	1.0	$1-0.2Ri$
σ_k	1.0	1.0	1.0	1.0
σ_ε	1.3	1.3	1.3	1.3
f_1	1.0	1.0	$1+0.15\exp\left(-\frac{R_t}{25}\right)$	1.0
f_2	$1-0.3\exp(-R_t^2)$	$1-0.3\exp(-R_t^2)$	$1-0.3\exp(-R_t^2)$	$1-0.3\exp(-R_t^2)$
F_μ	$\exp\left\{\frac{-3.4}{(1-R_t/50)^2}\right\}$	$\left\{1-\exp\left(-\frac{R_\tau}{26.5}\right)\right\}^2$	$\left\{1-\exp\left(-\frac{R_\tau}{26.5}\right)\right\}^2$	$\exp\left\{\frac{-3.4}{(1-R_t/50)^2}\right\}$
D	$-2\nu\left(\frac{\partial\sqrt{k}}{\partial r}\right)^2$	$-2\nu\left(\frac{\partial\sqrt{k}}{\partial r}\right)^2$	$-2\nu\left(\frac{\partial\sqrt{k}}{\partial r}\right)^2$	$-2\nu\left(\frac{\partial\sqrt{k}}{\partial r}\right)^2$
E	$2\nu\nu_t\left(\frac{\partial^2\bar{u}}{\partial r^2}\right)^2$	$\nu\nu_t(1-f_\mu)\left(\frac{\partial^2\bar{u}}{\partial r^2}\right)^2$	$\nu\nu_t(1-f_\mu)\left(\frac{\partial^2\bar{u}}{\partial r^2}\right)^2$	$2\nu\nu_t\left(\frac{\partial^2\bar{u}}{\partial r^2}\right)^2$

Numerical method

A control volume *finite*-difference technique[16] is employed to discretize the governing equations. The convergence criterion is set at:

$$\max\left|\frac{\phi^M-\phi^{M-1}}{\phi_{\max}^{M-1}}\right|<10^{-4} \tag{15}$$

for all the variables $\phi(\bar{u}, k, \text{and } \varepsilon)$. The superscripts M and $M-1$ in (15) indicate two successive iterations, while the subscript 'max' refers to a maximum value over the entire fields of iterations. Non-uniform cross-stream grids are used in which the radial mesh size is increased in a geometric ratio from the wall towards the centreline. The maximum mesh size is kept within 3% or $d/2$. The numbers of typical control volumes in the radial direction are 42 at $Re = 10{,}000$ and 62 at $Re = 20{,}000$. To ensure the accuracy of calculated results, at least two control volumes are always located in the viscous sublayer. Throughout the numerical calculations, the number of control volumes is properly selected between 42 and 78 to ensure validation of the numerical procedures and to obtain grid-independent results. It was confirmed that within this change of grid spacing the maximum relative error over all dependent variables was within 1%. The parameters used in the present study are Reynolds numbers $Re = 10{,}000$ and 20,000, velocity ratios $N = 0.0 \sim 2.0$, and Prandtl number $Pr = 0.7$ (air). The CPU time required in this scheme was about 10 to 100 min on a NEC personal computer (32 bit), depending on the number of meshes used and the calculation condition.

RESULTS AND DISCUSSION

Figure 2 illustrates the numerical results for the friction coefficient, f/f_0, at $Re = 10{,}000$ and 20,000, obtained using the models of Launder and Sharma[14], Nagano and Hishida[15], Torii *et al.*[13] and Launder *et al.*[6]. The experimental data of Kikuyama *et al.*[8] are superimposed for comparison. It is observed that the measured value of f/f_0 decreases gradually with an increase in the velocity ratio of a rotating pipe to fluid flow, N. This tendency is amplified with an increase in the Reynolds number. In general, the models of Launder and Sharma[14], Magano and Hishida[15]

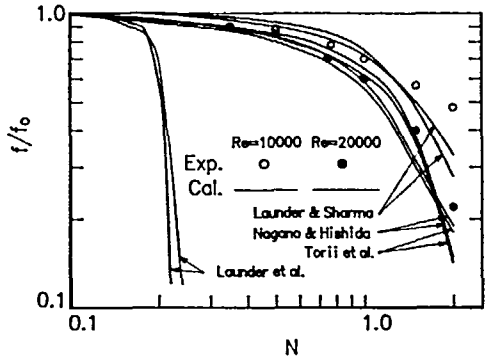

Figure 2 Predicted friction coefficients in a circular pipe rotating around its axis for Re = 10,000 and 20,000

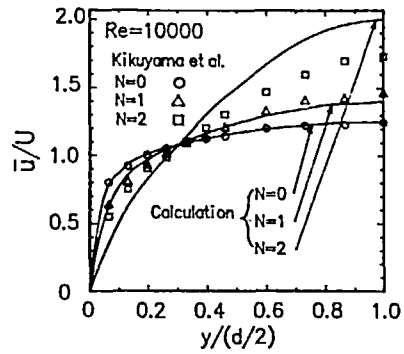

Figure 3 Variation of time-averaged streamwise velocity profiles with velocity ratios using the k–ε model of Torii *et al.*[13] for Re = 10,000

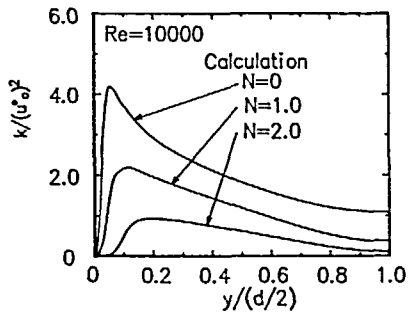

Figure 4 Variation of turbulent kinetic energy profiles with velocity ratios in the k–ε model of Torii *et al.*[13] for Re = 10,000

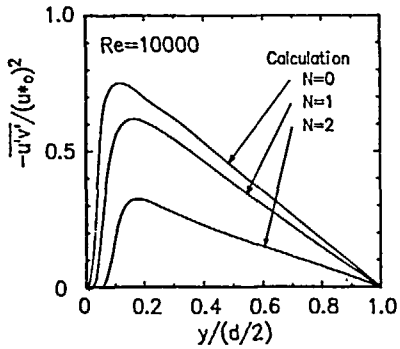

Figure 5 Variation of Reynolds stress profiles with velocity ratios in the k–ε model of Torii *et al.*[13] for Re = 10,000

and Torii *et al.*[13] predict to a certain degree experiments up to $N = 1.0$. It is seen that for $N < 1$, the three models yield lower values of f/f_0 for lower Reynolds numbers, opposite to the experimental results. This reversal can be partly attributed to the optimization of C_3, suggesting a need for future improvement in prediction accuracy. On the contrary, the model of Launder *et al.*[6] is valid only for small values of N. One may thus conclude that (i) the axial rotation of the pipe causes an attenuation in the friction coefficient, and (ii) flow behaviour can be described by the k–ε models proposed with a modification in the model function, (14), to include the swirling effect in the ε equation.

In order to explore the mechanisms of turbulent swirling flows in an axially rotating pipe, numerical results for the streamwise velocity, turbulent kinetic energy and Reynolds stress for Re = 10,000 are obtained. The following results are evaluated using the k–ε model of Torii *et al.*[13], with the other models producing similar results. *Figure 3* depicts the radial profiles of the calculated time-averaged streamwise velocity, $\bar{u}/U$, superposed with the experimental results of Kikuyama *et al.*[17]. The velocity ratio, $N(=W/U)$, is varied. $N = 0$ corresponds to no rotation case. An increase in N implies a raise in the rotational speed at a given axial velocity. It is observed that the velocity gradient at the wall, or equivalently wall shear stress, is reduced with

an increase in N. This behaviour is confirmed by experiments for $N = 0$ and 1 cases. In the $N = 2$ case, however, the model predicts a parabolic profile of the time-averaged axial velocity. It underpredicts $\bar{u}/U$ in the wall region and overpredicts in the core region. The turbulent kinetic energy k is normalized by the square of the friction velocity, u_0^*, for the pipe flow in the absence of rotation. The distribution of turbulent kinetic energy in the pipe cross-section is illustrated in *Figure 4* as a function og N for $Re = 10{,}000$. It is observed that in the absence of rotation, the turbulent kinetic energy undergoes a *sharp* rise in the wall region followed by a gradual decline towards the pipe centre. As N increases, the bump is reduced with its peak shifting toward the pipe centre. This behaviour is in accord with the variation of the streamwise velocity distribution in *Figure 3*. The change in the Reynolds stress profiles with rotation (i.e. N) is depicted in *Figure 5*. It is observed that the Reynolds stress level is reduced with an increase in N. The similar result is reported by Kawamura and Mishima[10].

In summary, when turbulent flow is introduced into an axially rotating pipe, the friction coefficient in the hydrodynamically, fully-developed downstream region is diminished caused by the axial rotation of the pipe. This trend is amplified with an increase in the velocity ratio. The mechanism is that in the region near the wall, a reduction in the velocity gradient induced by a pipe rotation suppresses the production of the turbulent kinetic energy and the Reynolds stress, resulting in a decrease in the friction coefficient.

CONCLUSIONS

Numerical simulation by means of four existing k–ε turbulence models has been employed to investigate the hydrodynamically, fully-developed isothermal flow in a pipe rotating around its axis. Consideration is given to the influence of the tangential-to-axial velocity ratio on the streamwise velocity distribution. The results are summarized as follows.

If the model function, (14), is introduced into the ε equation to include the swirling effect, the modified k–ε models can predict a reduction in the friction coefficient with an increase in the velocity ratio. The k–ε model of Torii *et al.*[13] predicts that an increase in the rotational speed results in a reduction in the velocity gradient at the pipe wall, the turbulent kinetic energy and Reynolds stress. It is disclosed that the turbulent kinetic energy in the wall region is substantially suppressed by the axial rotation of the pipe, resulting in an attenuation in the friction coefficient.

REFERENCES

1 Murakami, M. and Kikuyama, K. Turbulent flow in axially rotating pipes, *Trans. ASME J. Fluid Eng.*, **102**, 97–103 (1980)
2 Yamada, Y., Imao, S. and Toyozumi, K. Turbulence and its structure in an axially rotating pipe flows, *Trans. JSME*, **51**(461B), 34–42 (in Japanese) (1985)
3 Cannon, J. N. and Kays, W. M. Heat transfer to a fluid flowing inside a pipe rotating about its longitudinal axis, *ASME J. Heat Transfer*, **92**, 135–139 (1969)
4 Koosinlin, M. L., Launder, B. E. and Sharma, B. I. Prediction of momentum, heat and mass transfer in swirling, turbulent boundary layers, *Trans. ASME*, (*C*), **96**, 204–209 (1974)
5 Aguilar, F. and Pierce, F. J. Numerical analysis of turbulent flow along an abruptly *rotating* cylinder, *Trans. ASME, J. Fluid Eng.*, **101**, 251–258 (1979)
6 Launder, B. E., Priddin, C. H. and Sharma, B. I. The calculation of turbulent boundry layers on spinning and curved surfaces, *Trans. ASME, J. Fluid Eng.*, **99**, 231–239 (1977)
7 Kikuyama, K., Murakami, M. and Nishibori, K. Development of three-dimensional turbulent boundary layer in an axially rotating pipe, *Trans. ASME, J. Fluid Eng.*, **105**, 154–160 (1983a)
8 Bradshaw, P. The analogy between streamline curvature and buoyancy in turbulent shear flow, *J. Fluid Mech.*, **36**, 177–191 (1969)
9 Hirai, S., Takagi, T. and Matumoto, M. Prediction of the laminarization phenomena in turbulent swirling flows, *Trans. JSME*, **52**(476B), 1608–1616 (in Japanese) (1986)

10 Kawamura, H. and Mishima, T. Numerical prediction of turbulent swirling flow in a rotating pipe by a two-equation model of turbulence (Fully developed swirling flow), *Trans. JSME*, **57**(536B), 1251–1256 (in Japanese) (1991)
11 Rodi, W. Examples of turbulence models for incompressible flow, *AIAA J.*, **20**, 872–879 (1982)
12 Weigand, B. and Beer, H. Fluid flow and heat transfer in an axially rotating pipe: the rotational entrance, *Third Int. Symp. Transport Phenomena, Dynamics and Design of Rotating Machinery*, **1**, 439–454 (1990)
13 Torii, S., Shimizu, A., Hasegawa, S. and Higasa, M. Laminarization of strongly heated gas flow in a circular tube (numerical analysis by means of a modified k–ε model), *JSME Int. J. (II)*, **33**, 538–547 (1990)
14 Launder, B. E. and Sharma, B. I. Application of the energy-dissipation model of turbulence to the calculation of flow near a spinning disk, *Lett. Heat Mass Transfer*, (1), 131–137 (1974)
15 Nagano, Y. and Hishida, M. Improved form of the *et al.* model for wall turbulent shear flows, *Trans. ASME*, (*D*), **109**, 156–160 (1987)
16 Patankar, S. V. *Numerical Heat Transfer and Fluid Flow*, Hemisphere, New York (1980)
17 Kikuyama, K., Murakami, M., Nishibori, K. and Maeda, K. Flow in an axially rotating pipe (a calculation of flow in the saturated region), *Bull. JSME*, **26**, 506–513 (1983b)

APPENDIX

Equation (3) is integrated with respect to r, resulting in:

$$\overline{v'w'} = \nu r \frac{\partial}{\partial r}\left(\frac{\bar{w}}{r}\right) \tag{A1}$$

Thus $\overline{v'w'}$ is identical with the molecular viscosity. Equations (3) and (5) are combined to produce:

$$\frac{\partial}{\partial r}\left\{ r^3(\nu + \nu_t)\frac{\partial\left(\frac{\bar{w}}{r}\right)}{\partial r}\right\} = 0 \tag{A2}$$

Upon an integration, it yields:

$$r\frac{\partial\left(\frac{w}{r}\right)}{\partial r} = \frac{C'}{r^2(\nu + \nu_t)} \tag{A3}$$

in which C' is an integration constant. Since the left term in (A3) cannot be infinite at $r = 0$, C' is set equal to zero, resulting in:

$$r\frac{\partial\left(\frac{\bar{w}}{r}\right)}{\partial r} = 0 \tag{A4}$$

Thus, it is found that the rotating fluid moves as a rigid body.